Correlated Mobility Fluctuations and Contact Effects in p-Type Organic Thin-Film Transistors

G. Giusi, O. Giordano, G. Scandurra, S. Calvi, G. Fortunato, M. Rapisarda, L. Mariucci, and C. Ciofi

***Abstract*— Low-frequency noise (LFN) has been used in order to gain insight into the physical properties of the materials involved in organic thin-film transistors (OTFTs) fabrication, often with contradictory results. Besides the physical origin of noise, contact effects on noise have been a source of concern and discussion. In this paper, we report on accurate LFN measurements in p-type staggered top-gate OTFTs over four decades of channel current, from the subthreshold to the strong accumulation region. The measured spectra follow a clear $1/f$ behavior attributed to the trapping/detrapping of channel charge carriers into interface and oxide defects, while the influence of noise sources at contacts is found to be negligible. However, contacts affect the measured noise by a nonnegligible differential resistance. Noise data are interpreted in the context of a multitrap correlated mobility fluctuations (CMFs) model, showing that noise is dominated by acceptor-like traps. Despite the low mobility ($\mu_{\text{eff}} \sim 2$ cm^2/V/s), the large scattering parameter ($\alpha \sim 10^7$ Vs/C) produces an increase of the noise at the higher currents due to CMFs. The product $\alpha\mu_{\text{eff}} \approx 2{\cdot}10^7$ cm^2/C, which measures the strength of CMFs, is similar to what was reported for a-Si:H and much higher with respect to crystalline silicon MOSFETs revealing a strong correlation between CMFs and the state of disorder of the active layer.**

***Index Terms*— Low-frequency noise (LFN), LFN measurements (LFNMs), organic thin-film transistor (OTFT), OTFT contacts.**

I. Introduction

ORGANIC thin-film transistors (OTFTs) are finding more and more space in the electronics market thanks to their applications in flexible, large-area, and disposable electronic devices [1]. Notwithstanding the considerable technological advances in this field, there is still much debate on the detailed conduction mechanism in these devices. Low-frequency noise measurements (LFNMs), coupled to more conventional investigation techniques, can possibly result in a significant contribution toward a better understanding of the charge carrier transport within these devices. LFNMs have been an invaluable tool in the characterization of MOSFETs based on crystalline silicon (c-Si), and have indeed been used quite extensively to understand the material properties (in particular, the defect density) and channel transport mechanisms [2]. Because of this success, low-frequency noise (LFN) models and measurement techniques developed for c-Si MOSFETs have been used, over the last decade, to interpret the measured noise in OTFTs. In all cases, it has been found a higher level of $1/f$ noise with respect to c-Si MOSFETs [3]–[16]. This result has been interpreted as a higher defect density of OTFTs with respect to c-Si MOSFETs, due to the disordered structure of OTFTs. There have been many efforts to understand the origins of $1/f$ noise in OTFTs and to establish causative relationships between $1/f$ behavior and device structural and material characteristics. In most cases, the measured data fit within the Hooge mobility fluctuation (MF) model [6]–[8], while, in other cases, the number fluctuation (NF) [9]–[11] has been used to interpret the measured noise. In the first case, the noise is (assumed to be) generated in the semiconductor, and is the result of the variability of the scattering cross section, which causes a statistical fluctuation in the mobility and, as a consequence, in the channel current. In the second case, the noise is (assumed to be) due to the statistical fluctuation of the number of charged carriers due to their trapping/detrapping into interface and oxide defects. However, often, the reported analysis suffered from the fact that the explored bias range was quite limited, seldom extending above two decades. This limitation could be one of the causes of such different interpretations. In [16], we investigated the noise properties of p-channel staggered top-gate OTFTs over four decades of drain current, from the subthreshold to the strong accumulation region. Thanks to a very high sensitivity measurement system (reported in this paper in Section II) and to the large explorer bias range, we found that the measured data can be interpreted in a broader noise context, where both NF and correlated MFs (CMFs) are considered (Section V). It should be pointed out that, in OTFTs, the LFN analysis is complicated by the nonnegligible influence of the contacts. It has been reported, in fact, that the contacts are responsible for additional fluctuations, which, in some cases and particularly for short channel devices, completely dominate the overall LFN at strong current intensity [6], [7], [13], [14]. In [16], we limited our attention to long channel devices ($L = 100$ μm) where we found, by a simplified analysis, that contact effects are negligible. In this paper, we devote large space to the investigation of the influence

Manuscript received November 17, 2015; accepted January 12, 2016. Date of publication January 28, 2016; date of current version February 23, 2016. This work was supported by the Ministero dell'Istruzione, dell'Università e della Ricerca within the National Program PON Research and Competitiveness 2007-2013 through the Project entitled Elettronica su Plastica per Sistemi Smart-Disposable under Grant PON02_00355_3416798. The review of this paper was arranged by Editor Y.-Y. Noh. *(Corresponding author: G. Giusi.)*

G. Giusi, O. Giordano, G. Scandurra, and C. Ciofi are with the Department of Engineering, University of Messina, Messina 98166, Italy (e-mail: ggiusi@unime.it; oraziomariagiordano@alice.it; gscandurra@unime.it; cciofi@unime.it).

S. Calvi, G. Fortunato, M. Rapisarda, and L. Mariucci are with the Institute for Microelectronics and Microsystems, National Research Council, Rome 00133, Italy (e-mail: sabrina.calvi@artov.imm.cnr.it; guglielmo.fortunato@cnr.it; matteo.rapisarda@cnr.it; luigi.mariucci@cnr.it).

Digital Object Identifier 10.1109/TED.2016.2518305

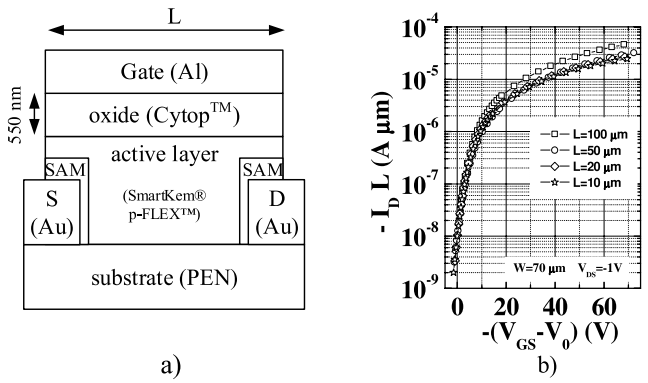

Fig. 1. (a) Device structure (not to scale) of the investigated OTFTs. (b) Typical current–voltage characteristic in OTFTs with $W = 70$ μm and for different gate length (L) in linear regime ($V_{\rm DS} = -1$ V).

of contacts on the measured noise (Section IV), extending the analysis to shorter channel devices (down to 10 μm). We found that, even in the shortest channel devices, the noise generated at the contacts is indeed negligible with respect to the intrinsic channel noise, while the effect of the differential contact resistance is relevant in the shorter channels.

II. Device Structure and Measurement Setup

OTFTs, with staggered top-gate configuration [Fig. 1(a)], were fabricated on flexible (125-μm thick) polyethylene-naphtalate (PEN, DuPont Teijin Teonex Q65HA) by using solution processed semiconductor and dielectric. The source and drain electrode metals were deposited by thermal evaporation of 25 nm of gold and defined by lift-off process. This process allows to obtain a lower contamination of the electrode surface. Prior to the deposition of a semiconductor layer, the source and drain contacts were pretreated by a self-assembled monolayer of 2,3,4,5,6-pentafluorobenzenethiol to optimize hole injection in the Highest Occupied Molecular Orbital level of organic semiconductor [17]. Organic semiconductor (OSC, SmartKem p-FLEX, 20-nm thick [18]) and amorphous fluoropolymer gate dielectric [poly(perfluorobutenylvinylether, Cytop) 550-nm thick, relative dielectric constant $\sim$2.1] were sequentially deposited via spin coating in air. After deposition, the semiconductor and dielectric layers were annealed at 100 °C on hot plate in air. Finally, Al gate electrodes (50-nm thick) were evaporated and defined by photolithography. It can be noted that OTFTs with a staggered structure usually show a lower contact resistance compared with coplanar devices [19], [20]. Indeed, it has been shown that in staggered devices, the carrier injection occurs, at low drain voltage, in the area where gate electrode overlaps the source and drain contacts, resulting in a low parasitic contact resistance. Investigated devices have a gate width $W = 70$ μm and gate length L ranging from 10 to 100 μm.

The experimental setup shown in Fig. 2 allows both dc and noise characterization [21]–[23]. Terminal bias is provided by the semiconductor parameter analyzer HP4155B. During dc operation, the switch S connects the source terminal to the HP4155B, while during noise measurement, the source is

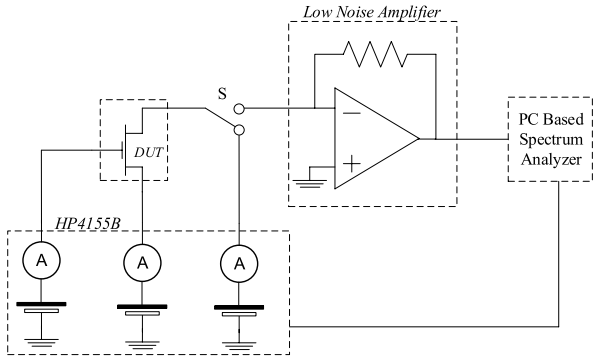

Fig. 2. Experimental setup for dc and noise characterization of OTFTs.

connected to the input of a transimpedance low-noise amplifier (LNA) that has been designed and built for this specific application. The LNA provides: 1) the 0 V bias to the source; 2) the conversion of channel current fluctuations into voltage fluctuations; and 3) sufficiently high signal-to-noise ratio for the successive elaboration based on the standard periodogram Discrete Fourier Transform analysis. The spectrum analyzer is composed of a PC equipped with a dynamic signal analyzer board (NI 4462). DC and noise measurement sequences are fully automated by the system software running on the PC. The configuration reported in Fig. 2 is properly suited for organic devices where large biases are commonly necessary. In fact, since the common mode voltage at the input of the LNA is 0 V independently on the bias, relative large biases can be applied to the device avoiding LNA saturation.

III. Basic DC and Noise Measurements

Fig. 1(b) shows the typical scaled drain current (I_D) versus gate voltage (V_G) with $V_{\rm DS} = -1$ V in OTFTs for different values of L measured during noise measurement with a delay time of 30 s. We found that $V_{\rm DS} = -1$ V is sufficiently small to consider even the shorter devices ($L = 10$ μm) in linear regime in all the bias range, from the subthreshold to the accumulation region. In order to address the device-to-device variability, we aligned the measured I–V curves in a bias point $V_G = V_0$, in the subthreshold region, where $I_D \cdot L = 10$ nA $\cdot$ μm. Fig. 1(b) shows that scaling the drain current by L is not sufficient to obtain the same current in devices with different values of L, especially in the accumulation region. As we will see in Section IV, this is the result of a series resistance. The measured mobility in devices with $L = 100$ μm (which are nearly free of contact effects [16]) is about 2 cm^2/V/s.

Noise measurements [16] show a clear $1/f^{\gamma}$, $\gamma \approx 1$, behavior observed in all the investigated measurement bias ranges. Since we obtain purely flicker noise, we can conclude that the noise is generated by a continuous distribution of defects. This is different from what is sometimes reported in the literature. Other works have, in fact, reported deviations from the pure $1/f$ spectrum that have been attributed to generation-recombination noise caused by traps at the grain boundaries of the active layer [11], [12]. Normally, noise data are reported as the normalized drain noise $S_{\rm ID}/I_D^2$ versus I_D, where $S_{\rm ID}$ is the power spectral density (PSD) of drain current fluctuations.

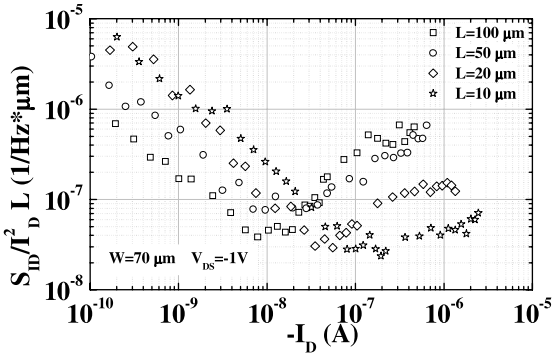

Fig. 3. Normalized device current PSD evaluated at $f = 1$ Hz as a function of the drain current ($-I_D$) for different channel lengths (L).

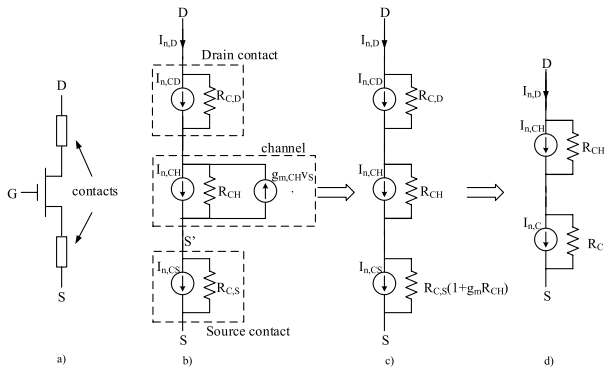

Fig. 4. (a) OTFT structure, including symmetrical contacts. (b)–(d) Equivalent noise models.

As the noise scales with the gate area, Fig. 3 shows $S_{\rm ID}/I_D^2 L$ versus I_D (at $f = 1$ Hz) in OTFTs with different values of L. It is apparent that the gate area scaling is not sufficient to get the same noise with different values of L. This result may be due to two reasons: 1) contact effects can play a significant role and 2) $S_{\rm ID}/I_D^2 L$ may not be solely a function of I_D, depending on noise mechanisms. As we shall discuss in Sections IV and V, in the investigated devices, the noise contribution from contacts can be considered negligible in all cases.

Contacts, however, have an effect on the measurements because of their nonnegligible differential resistance. The measured noise can be interpreted as caused by defects at the semiconductor–oxide interface and in the oxide, which cause fluctuations in the number of charge carriers and correlated fluctuations of the scattering cross section. In this CMF context, $S_{\rm ID}/I_D^2 L$ is a function of I_D/g_m and not of I_D alone.

IV. Contact Effects on Noise

It has been reported that the junctions between the organic semiconductor and source/drain contacts [Fig. 4(a)] can be preferential defect sites that generate additional fluctuations. Moreover, the differential contact resistance also affects the measured noise [6], [7], [13], [14]. Therefore, before processing noise data to extract defect parameters, it is necessary to estimate the influence of contacts on the measured noise. Fig. 4(b) shows the equivalent noise model of the OTFT. The intrinsic transistor is schematized with the channel differential resistance $R_{\rm CH}$ and a current noise generator $I_{n,\rm CH}$ responsible of the intrinsic fluctuations originated in the channel. Source and drain contacts are schematized with two physical current noise generators, including the differential resistances and current noise generators responsible of fluctuations originated in the contact regions. Since the intrinsic source (S') is not grounded, the current noise generator $g_{m,\rm CH}v'_S$ must be, in principle, considered. The intrinsic transconductance $g_{m,\rm CH}(=dI_D/dV_{\rm GS'})$ is different from the measured transconductance $g_m(=dI_D/dV_{\rm GS})$ as $g_{m,\rm CH} = g_m/(1-g_m R_{C,S})$. However, due to the low mobility, we found that $g_m R_{C,S} \ll 1$, so that $g_{m,\rm CH} \approx g_m$. It can be simply demonstrated that the effect of the current noise generator $g_{m,\rm CH}v_S$ can be resumed as an effective increase of the source resistance $R_{C,S}(1+g_m R_{\rm CH})$, as shown in Fig. 4(c). However, due to the low mobility, $g_m R_{\rm CH} \ll 1$, so that, from a practical point-of-view, the effect of $g_{m,\rm CH}v'_S$ is not relevant. The two contacts can then be schematized as a single current noise generator, as shown in Fig. 4(d), where R_C is the total contact resistance. The measured drain current fluctuations are

$$I_{n,D} = I_{n,\rm CH}\frac{R_{\rm CH}}{R_T} + I_{n,C}\frac{R_C}{R_T} \tag{1}$$

where $R_T = R_{\rm CH} + R_C$ is the total differential device resistance. The measured noise ($\rm A^2/Hz$) is then

$$S_{\rm ID} = S_{I,\rm CH}\frac{R_{\rm CH}^2}{R_T^2} + S_{I,C}\frac{R_C^2}{R_T^2} \tag{2}$$

where $S_{I,\rm CH}$ is the current PSD associated with $I_{n,\rm CH}$ and $S_{I,C}$ is the current PSD associated with $I_{n,C}$. Since we are interested in the intrinsic noise component $S_{I,\rm CH}$, we have to evaluate the impact of the differential contact resistance (R_C) and of the contact noise ($S_{I,C}$).

A. Differential Contact Resistance

The total differential device resistance is a function of the bias point and can be calculated from I–V curves as $R_T = (\partial i_D/\partial v_{\rm DS}|_{\rm VGS,VDS})^{-1}$ where $V_{\rm GS}$ and $V_{\rm DS}$ are the voltages applied at the gate and drain terminals with respect to the source, respectively. In the linear region $R_T(V_{\rm GS}) \approx V_{\rm DS}/I_D$, R_T, $R_{\rm CH}$, and R_C are independent of $V_{\rm DS}$ and are dependent on $V_{\rm GS}$ only. In particular, R_C does not depend on the channel length L. In this paper, all noise measurements have been done with $V_{\rm DS} = -1$ V, which is sufficiently small to consider the investigated devices with $L \geq 10$ μm in the linear region. Since $R_{\rm CH} \propto 1/I_D \propto L$, while R_C is expected to be independent on L, the contact resistance can be extracted by the linear extrapolation of R_T measured in devices with different values of L at the same gate voltage overdrive. Following this shrewdness, we can compare R_T in different devices at the same gate overdrive condition. Fig. 5 (top) shows the linear fit of the curve $R_T(L)$ in a bias point in the strong accumulation region ($V_{\rm GS}$–$V_0 = -60$ V) with L ranging from 10 to 100 μm.

The linear behavior has been observed in all bias points, from the subthreshold to the strong accumulation region. Let us notice that the measured linear dependence of

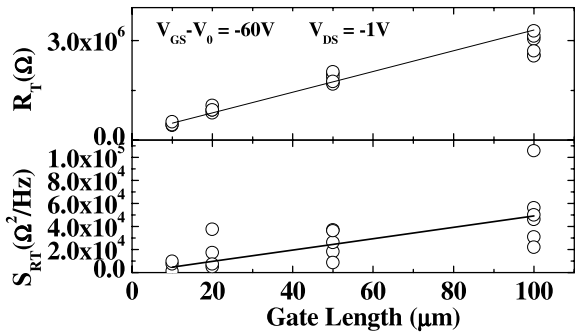

Fig. 5. Top: linear fit of the curve $R_T(L)$ in order to extract R_C. Bottom: contact noise extrapolation from total resistance noise as a function of L.

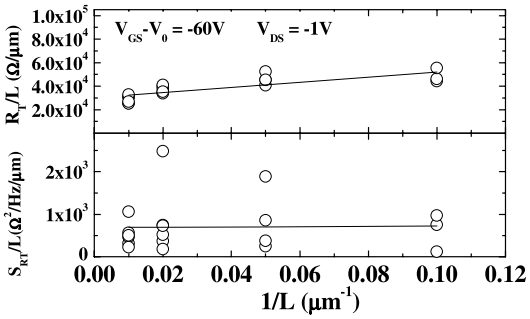

Fig. 6. Top: linear fit of the curve $R_T/L(1/L)$ in order to extract R_C. Bottom: contact noise extrapolation from total resistance noise as a function of L.

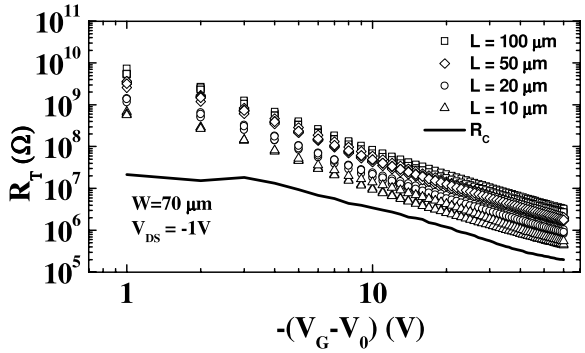

Fig. 7. Symbols: total resistance as a function of gate voltage overdrive for different samples with the same nominal channel length (L). Solid line: contact resistance (R_C) calculated by linear extrapolation [Fig. 6 (top)].

R_T on L indicates that the alignment process has been successful. However, due to the dispersion in the measured data, a more robust procedure to extract R_C is the linear fit of R_T/L versus $1/L$ [15], as shown in Fig. 6 (top). The clear positive slope of the curve $R_T/L(1/L)$ confirms that a nonnegligible differential contact resistance is present in the investigated devices. In particular, in the considered bias point (V_{GS}–$V_0 = -60$ V), we found $R_C \sim 200$ kΩ. Fig. 7 shows the total resistance and the extrapolated contact resistance as a function of the gate overdrive (V_{GS}–V_0). The contact resistance reduces with the gate overdrive from $\sim 10^7$ Ω in the subthreshold region to $\sim 10^5$ Ω in accumulation. A similar behavior and order of magnitude for R_C have been already reported in [15]. As evident from Fig. 7, the total resistance in the shorter channel devices is significantly affected by R_C, especially in the strong accumulation region, while R_C is almost negligible in the subthreshold region. However, in longer channel devices, for instance $L = 100$ μm, the contribution coming from R_C can be, to a first approximation, neglected, since $R_T \gg R_C$.

B. Contact Noise

In order to estimate the impact of the contact noise $S_{I,C}$, (2) can be written as

$$S_{\mathrm{RT}} = S_{\mathrm{RCH}} + S_{\mathrm{RC}}$$
$$S_{\mathrm{RT}} = \frac{S_{\mathrm{ID}}}{I_D^2} R_T^2 \quad S_{\mathrm{RCH}} = \frac{S_{I,\mathrm{CH}}}{I_D^2} R_{\mathrm{CH}}^2 \quad S_{\mathrm{RC}} = \frac{S_{I,C}}{I_D^2} R_C^2 \qquad (3)$$

where S_{RT}, S_{RCH}, and S_{RC} are the PSD (Ω^2/Hz) related to R_T, R_{CH}, and R_C fluctuations, respectively. As in the case of c-Si MOSFETs, it is reasonable to assume that the intrinsic equivalent gate voltage noise ($S_{\mathrm{VG,CH}}$) is averaged as the gate area increases, that is $S_{\mathrm{VG,CH}} \propto 1/(\mathrm{WL})$. Since $S_{R,\mathrm{CH}} = S_{\mathrm{VG,CH}} R_{\mathrm{CH}}^2/(I_D/g_m)^2$, it follows that $S_{R,\mathrm{CH}} \propto L$. The physical origin of the contact noise (S_{RC}) is an argument still not clear. If S_{RC} was only due to the dc resistance of the path that the carriers have to travel to reach the contact, as in the case of c-Si MOSFETs, S_{RC} would be thermal noise (except at very low frequencies) and would not be measurable because the observed noise is flicker. If a significant S_{RC} contribution is present, it has the same frequency dependence of S_{RCH}, that is $1/f$. The physical origin of this $1/f$ noise could be due to the defects in the organic semiconductor away from the channel and close to the contacts. Drain current fluctuations could be, therefore, due to individual trapping/detrapping Random Telegraph Noise processes leading to an overall $S_{\mathrm{IC}} \propto I_D^2$. Since R_C is independent of L, from (3), also the flicker component of S_{RC} is independent of L, that is constant. Since $S_{R,\mathrm{CH}} \propto L$ and S_{RC} is constant, S_{RC} can be extrapolated by the linear fit of the curve S_{RT} versus L [14]. Fig. 5 (bottom) shows the measured S_{RT} as a function of L in a bias point in the strong accumulation region (V_{GS}–$V_0 = -60$ V) with L ranging from 10 to 100 μm. Notwithstanding the large data dispersion, it is possible to recognize the expected linear dependence of S_{RT} on L. However, due to the large data dispersion, a more robust procedure to extrapolate S_{RC} is the liner fit S_{RT}/L versus $1/L$ [14]. Fig. 6 (bottom) shows that the slope of S_{RT}/L versus $1/L$ is almost zero meaning that S_{RC} appears to be negligible with respect to S_{RCH} ($S_{\mathrm{RC}} \ll S_{\mathrm{RCH}}$), so that $S_{RT} \propto L$. Fig. 8 shows S_{RT}/L in all investigated devices as a function of the gate overdrive. The noise S_{RT} scales well with L, except for a nonnegligible data dispersion, confirming that $S_{\mathrm{RC}} \ll S_{\mathrm{RCH}}$ in the whole bias range. In other works, significant effects of S_{RC} have been reported in both staggered [13] and coplanar [14] OTFTs, possibly resulting in a nonnegligible defect density in the contact region due to different materials and/or processes.

V. Contact-Free Noise Measurements

In this section, we will analyze contact-free noise data as a function of the bias point in order to get understanding on

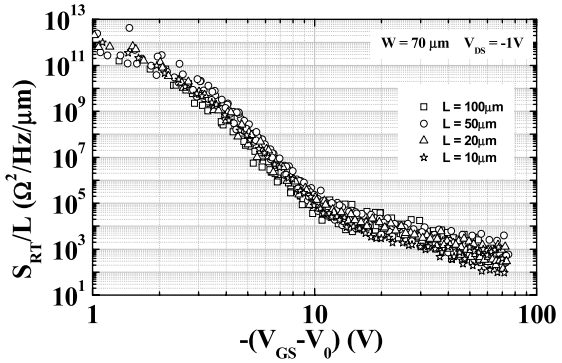

Fig. 8. Scaled total device resistance PSD as a function of gate voltage overdrive for different samples with different values of L.

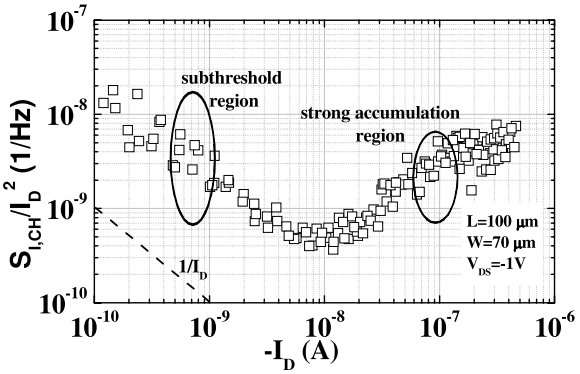

Fig. 9. Normalized channel drain current PSD evaluated at $f = 1$ Hz as a function of the drain current ($-I_D$) in four samples with $L = 100$ μm.

the physical origin of noise. Most of results have been already discussed in [16] and reported here for completeness, except for the fact that, here, the investigation is extended to a short channel device considering contact effects. From the analysis developed in Section IV, it is apparent that, in all the explored bias range from the subthreshold to the strong accumulation regime, the contact noise S_{RC} can be neglected, while it is necessary to consider the contact resistance R_C, especially in the shorter channel devices. Once that S_{ID} and I_D have been measured, and R_C extrapolated as discussed in Section IV, the intrinsic normalized drain current PSD can be evaluated from (2) and (3)

$$\frac{S_{I,\mathrm{CH}}}{I_D^2} \approx \frac{S_I}{I_D^2}\left(\frac{R_T}{R_T - R_C}\right)^2. \tag{4}$$

As already stated in Section I, the measured noise in OTFTs has been attributed to Hooge MFs in some cases, while it has been attributed to carrier NFs in some other cases. If the noise is dominated by MFs, then $S_{\mathrm{ICH}}/I_D^2 \propto 1/I_D$, while, if it is dominated by NFs, then $S_{\mathrm{VG,CH}} = S_{\mathrm{ICH}}/g_m^2$ is constant with respect to the bias. Checking these dependencies is a common method to discriminate the origin of noise. Fig. 9 shows the normalized channel current PSD (S_{ICH}/I_D^2) over four decades of drain current (from subthreshold to strong accumulation region) in devices with $L = 100$ μm biased in liner regime. Two different trends are observed in the subthreshold and in the strong accumulation regimes, respectively. This is somewhat different from other reports, where a monotonic decrease of the normalized noise is observed [10], [13], [14]. We want to remark that the result found by other authors can be affected by the limited explored bias range. In the subthreshold region, the measured normalized noise is almost proportional to $1/I_D$, suggesting that Hooge MFs could be at the origin of the measured current fluctuations. However, in the accumulation region, the noise changes behavior increasing with $-I_D$ and showing a minimum around 10 nA. This behavior is neither consistent with MFs nor with carrier NFs, since in that case $S_{\mathrm{ICH}}/I_D^2 \propto (g_m/I_D)^2$ (that is the normalized noise reduces as the drain current increases).

Besides classical MFs and NFs, noise in MOSFETs has also been interpreted in a larger context by means of a correlated NF–MF theory [24]. CMFs are different from Hooge MFs as they are due to the statistical fluctuation of the scattering cross section induced by the fluctuation of oxide charge which, in turn, is due to trapping/detrapping of charged carriers. For this reason, the MFs are correlated with NFs. In the case of a pMOSFETs, the model is

$$S_{\mathrm{VG,CH}} = S_{\mathrm{VFB}}\left[1 \pm \alpha\mu_{\mathrm{eff}} C_{\mathrm{ox}}\left(-\frac{I_D}{g_m}\right)\right]^2$$
$$S_{\mathrm{VFB}} = \frac{kTq^2}{8WLC_{\mathrm{ox}}^2}\frac{N_T(E_F)/\lambda}{f} \quad \alpha = \frac{1}{\mu_{\mathrm{eff}}^2}\left|\frac{\partial\mu_{\mathrm{eff}}}{\partial Q_{\mathrm{ox}}}\right| \tag{5}$$

where $S_{\mathrm{VG,CH}}$ is the PSD (V^2/Hz) related to the equivalent gate voltage fluctuations, S_{VFB} is the flat-band gate voltage PSD, μ_{eff} is the effective mobility in the active layer, Q_{ox} is the oxide charge density, α is a scattering parameter, k is the Boltzmann constant, T is the absolute temperature, q is the elementary charge, C_{ox} is the oxide capacitance, $N_T(E_F)$ is the trap density corresponding to the oxide energy level aligned with the Fermi level (E_F) in the active layer, and λ is the tunneling parameter. The scattering parameter α considers for oxide-induced MFs. In the CMF model, $S_{\mathrm{VG,CH}}$ is a quadratic function of the ratio I_D/g_m. In the case of donor traps [sign + in (5)], $S_{\mathrm{VG,CH}}$ increases with $-I_D/g_m (>0$, for pFETs), while in the case of acceptor traps [sign − in (5)], $S_{\mathrm{VG,CH}}$ has a minimum, which is also a zero, with respect to $-I_D/g_m$. However, a zero in the measured noise is not possible from a physical point-of-view and it is necessary to admit a distribution of more dominant trap species, each of which is characterized by a couple of parameters N_{Ti} and α_i. In fact, if more trap species contribute to drain current fluctuations, the total $S_{\mathrm{VG,CH}}$ can be calculated as the sum of the individual $S_{\mathrm{VG,CHi}}$, because trapping/detrapping processes are uncorrelated. Since each $S_{\mathrm{VG,CHi}}$ is a quadratic form, the total $S_{\mathrm{VG,CH}}$ is also a quadratic form. Fig. 10 shows the extrapolated $S_{\mathrm{VG,CH}}$ versus I_D/g_m in devices with different values of L from 10 to 100 μm. In order to compare devices with different values of L, since the noise is expected to scale with gate area, the intrinsic gate voltage PSD is multiplied by the nominal channel length L ($S_{\mathrm{VG,CH}} \cdot L$).

Fig. 10 shows a second-order polynomial fit, which is in good agreement with the measured data. The measured data show a minimum, so that they can be interpreted in a multitrap CMF context as discussed above. The presence

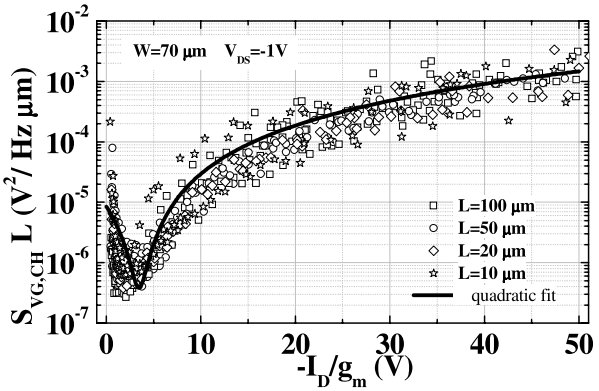

Fig. 10. Symbols: $S_{\mathrm{VG,CH}}L$ evaluated at $f = 1$ Hz as a function of $-I_D/g_m$ in OTFTs with different values of L. Solid line: quadratic fit according to the CMF model (5).

of the minimum allows us to conclude that acceptor traps contribute to $S_{\mathrm{VG,CH}}$ in the subthreshold region, where $S_{\mathrm{VG,CH}}$ decreases. However, we cannot exclude the presence of donor traps. In the strong accumulation region, it is possible to make a linear fit of $S_{\mathrm{VG,CH}}^{1/2}$ with respect to $-I_D/g_m$, meaning that, in this region, the noise is mostly due to single dominant trap species. Following this fitting procedure we obtained, from the statistical analysis of the different devices, the averages values of $N_T' = N_T/\lambda = 3.2 \cdot 10^{12}$ cm^{-2}eV^{-1} and $\alpha = 1.6 \cdot 10^7$ Vs/C [with the sign $-$ in (5)]. The extracted trap density is in line with [10] and [11], and it is much higher (assuming the same λ) with respect to the conventional MOSFETs. The sign $-$ in (5) means that, as in the subthreshold region, the noise in the strong accumulation region is dominated by acceptor traps. The scattering parameter value is much higher with respect to the case of (p- and n-type) MOSFETs ($\sim 10^7$ versus 10^4 Vs/C). However, the strength of CMFs is proportional to the value of the product $\alpha\mu_{\mathrm{eff}}$. It can be noted that similar $\alpha\mu_{\mathrm{eff}}-$ values found from the present analysis ($\alpha\mu_{\mathrm{eff}} \sim 3 \cdot 10^7$ cm^2/C) have been reported for a-Si:H TFTs [25] ($\alpha\mu_{\mathrm{eff}} = 2 \cdot 10^7$ cm^2/C) and are much higher with respect to the case of c-Si MOSFETs, although the mobility in c-Si MOSFETs is much higher than in OTFTs. These comparisons suggest a correlation between the state of order of the active layer and the relevance of CMFs. Finally, it is important to stress that the raise of noise in Fig. 9 is only due to CMFs and not due to contact effects, as they have been considered following the procedure in Section IV.

VI. Conclusion

In this paper, we have presented accurate LFNMs in staggered top-gate OTFTs over four orders of drain current, from the subthreshold to the strong accumulation region. Observed LFN spectra are $1/f$ in all the investigated bias and frequency ranges. This is different to what sometimes reported by other works where deviations from the pure $1/f$ spectrum have been observed. The measured noise is not affected by contact noise (differently to what reported in other works), is affected by the differential contact resistance, and is caused by acceptor-like defects at the semiconductor–oxide interface and in the oxide, which cause fluctuations in the number of charge carriers and correlated fluctuations of the scattering cross section. The extrapolated trap density and scattering parameter α are much higher with respect to what measured in c-Si MOSFETs. Despite the low mobility, the large α produces an increase of the noise at the higher currents due to CMFs. The product $\alpha\mu_{\mathrm{eff}}$, which measure the strength of CMFs, is similar to what reported for a-Si:H and much higher with respect to c-Si MOSFETs, revealing a strong correlation between CMFs and the state of disorder of the active layer.

References

[1] O. Marinov, M. J. Deen, and B. Iniguez, "Charge transport in organic and polymer thin-film transistors: Recent issues," *IEE Proc.-Circuits, Devices Syst.*, vol. 152, no. 3, pp. 189–209, Jun. 2005.

[2] A. Van der Ziel, *Noise in Solid State Devices and Circuits*. New York, NY, USA: Wiley, 1986, p. 145.

[3] Y. Xu *et al.*, "Understanding thickness-dependent charge transport in pentacene transistors by low-frequency noise," *IEEE Electron Device Lett.*, vol. 34, no. 10, pp. 1298–1300, Oct. 2013.

[4] Y.-H. Tai, C.-Y. Chang, C.-L. Hsieh, Y.-H. Yang, W.-K. Chao, and H.-E. Chen, "Dependence of the noise behavior on the drain current for thin film transistors," *IEEE Electron Device Lett.*, vol. 35, no. 2, pp. 229–231, Feb. 2014.

[5] Z. Jia, I. Meric, K. L. Shepard, and I. Kymissis, "Doping and illumination dependence of $1/f$ noise in pentacene thin-film transistors," *IEEE Electron Device Lett.*, vol. 31, no. 9, pp. 1050–1052, Sep. 2010.

[6] P. V. Necliudov, S. L. Rumyantsev, M. S. Shur, D. J. Gundlach, and T. N. Jackson, "$1/f$ noise in pentacene organic thin film transistors," *J. Appl. Phys.*, vol. 88, no. 9, pp. 5395–5399, 2000.

[7] L. K. J. Vandamme, R. Feyaerts, G. Trefán, and C. Detcheverry, "$1/f$ noise in pentacene and poly-thienylene vinylene thin film transistors," *J. Appl. Phys.*, vol. 91, no. 2, pp. 719–723, 2002.

[8] O. Marinov, M. J. Deen, J. Yu, G. Vamvounis, S. Holdcroft, and W. Woods, "Low-frequency noise in polymer thin-film transistors," *IEE Proc.-Circuits, Devices Syst.*, vol. 151, no. 5, pp. 466–472, Oct. 2004.

[9] S. Martin *et al.*, "Flicker noise properties of organic thin-film transistors," *J. Appl. Phys.*, vol. 87, no. 7, pp. 3381–3385, 2000.

[10] Y. Xu, T. Minari, K. Tsukagoshi, J. Chroboczek, F. Balestra, and G. Ghibaudo, "Origin of low-frequency noise in pentacene field-effect transistors," *Solid-State Electron.*, vol. 61, no. 1, pp. 106–110, 2011.

[11] C. Y. Han, L. X. Qian, C. H. Leung, C. M. Che, and P. T. Lai, "A low-frequency noise model with carrier generation-recombination process for pentacene organic thin-film transistor," *J. Appl. Phys.*, vol. 114, no. 4, p. 044503, 2013.

[12] H. Kang, L. Jagannathan, and V. Subramanian, "Measurement, analysis, and modeling of $1/f$ noise in pentacene thin film transistors," *Appl. Phys. Lett.*, vol. 99, no. 6, p. 062106, 2011.

[13] Y. Xu *et al.*, "Diagnosis of low-frequency noise sources in contact resistance of staggered organic transistors," *Appl. Phys. Lett.*, vol. 98, no. 3, p. 033505, 2011.

[14] Y. Xu *et al.*, "Extraction of low-frequency noise in contact resistance of organic field-effect transistors," *Appl. Phys. Lett.*, vol. 97, no. 3, p. 033503, 2010.

[15] Y. Xu, R. Gwoziecki, I. Chartier, R. Coppard, F. Balestra, and G. Ghibaudo, "Modified transmission-line method for contact resistance extraction in organic field-effect transistors," *Appl. Phys. Lett.*, vol. 97, no. 6, p. 063302, 2010.

[16] G. Giusi *et al.*, "Evidence of correlated mobility fluctuations in p-type organic thin-film transistors," *IEEE Electron Device Lett.*, vol. 36, no. 4, pp. 390–392, Apr. 2015.

[17] D. Boudinet *et al.*, "Modification of gold source and drain electrodes by self-assembled monolayer in staggered n- and p-channel organic thin film transistors," *Organic Electron.*, vol. 11, no. 2, pp. 227–237, 2010.

[18] M. A. Cowin, R. Griffiths, and K. Crowley, "Advances in high performance organic semiconductors for flexible displays," in *12th Int. Meeting Inf. Display (IMID) Dig.*, 2012, pp. 154–155.

[19] L. Mariucci, M. Rapisarda, A. Valletta, S. Jacob, M. Benwadih, and G. Fortunato, "Current spreading effects in fully printed p-channel organic thin film transistors with Schottky source–drain contacts," *Organic Electron.*, vol. 14, no. 1, pp. 86–93, 2013.

[20] C. H. Kim, Y. Bonnassieux, and G. Horowitz, "Fundamental benefits of the staggered geometry for organic field-effect transistors," *IEEE Electron Device Lett.*, vol. 32, no. 9, pp. 1302–1304, Sep. 2011.

[21] G. Giusi, O. Giordano, G. Scandurra, C. Ciofi, M. Rapisarda, and S. Calvi, "Automatic measurement system for the DC and low-f noise characterization of FETs at wafer level," in *Proc. IEEE Int. Instrum. Meas. Technol. Conf. (I2MTC)*, May 2015, pp. 2095–2100.

[22] G. Giusi, F. Crupi, C. Ciofi, and C. Pace, "Instrumentation design for gate and drain low frequency noise measurements," in *Proc. IEEE IMTC Conf.*, Apr. 2006, pp. 1747–1750.

[23] G. Giusi, G. Scandurra, and C. Ciofi, "Estimation errors in $1/f^{\gamma}$ noise spectra when employing DFT spectrum analyzers," *Fluctuation Noise Lett.*, vol. 12, no. 1, p. 1350007, 2013.

[24] G. Ghibaudo, O. Roux, C. Nguyen-Duc, F. Balestra, and J. Brini, "Improved analysis of low frequency noise in field-effect MOS transistors," *Phys. Status Solidi A*, vol. 124, no. 2, pp. 571–581, 1991.

[25] E. G. Ioannidis, A. Tsormpatzoglou, D. H. Tassis, C. A. Dimitriadis, F. Templier, and G. Kamarinos, "Characterization of traps in the gate dielectric of amorphous and nanocrystalline silicon thin-film transistors by $1/f$ noise," *J. Appl. Phys.*, vol. 108, no. 10, p. 106103, 2010.

Authors' photographs and biographies not available at the time of publication.